

1 **NLRP3 controls ATM activation in response to DNA damage.**

2

3 Mélanie BODNAR-WACHTEL^{a,b,c,d,#}, Anne-Laure HUBER^{a,b,c,d,#}, Julie GORRY^{a,b,c,d}, Sabine
4 HACOT^{a,b,c,d}, Laetitia GEROSSIER^{a,b,c,d}, Baptiste GUEY^{a,b,c,d}, Nadège GOUTAGNY^{a,b,c,d},
5 Birke BARTOSCH^{a,b,c,d}, Elise BALLOT^e, François GHIRINGHELLI^e, Bénédicte F. PY^f,
6 Yohann COUTE^g, Annabelle BALLESTA^h, Sylvie LANTUEJOUL^{d,i}, Janet HALL^{a,b,c,d}, and
7 Virginie PETRILLI^{a,b,c,d*}.

8

9 ^a INSERM U1052, Centre de Recherche en Cancérologie de Lyon, F-69000 Lyon, France; ^b
10 CNRS UMR5286, Centre de Recherche en Cancérologie de Lyon, F-69000 Lyon, France; ^c
11 Université de Lyon, Université Lyon 1, F-69000 Lyon, France ; ^d Centre Léon Bérard, F-
12 69008 Lyon, France; ^e INSERM 1231, University of Burgundy, Department of Medical
13 Oncology, France; ^f CIRI, Centre International de Recherche en Infectiologie, Univ Lyon,
14 INSERM, U1111, Université Claude Bernard Lyon 1, CNRS, UMR5308, ENS de Lyon, F-
15 69000 Lyon, France; ^g University Grenoble Alpes, CEA, Inserm, IRIG, BGE, 38000
16 Grenoble, France ; ^h INSERM and Paris Sud University, UMRS 935, Campus CNRS,
17 Villejuif, F-94807, France. & Honorary position, University of Warwick, UK; ⁱ Département
18 de Pathologie, Pôle de Biologie et de Pathologie, Centre Hospitalier Universitaire, Inserm
19 U823, Institut A Bonniot-Université J Fourier, Grenoble, France. # contributed equally.

20 Corresponding Author: virginie.petrilli@lyon.unicancer.fr

21

22 **Running title:** NLRP3 controls ATM activation

23

24 The authors declare no potential conflict of interest.

25

26 **ABSTRACT**

27

28 The DNA damage response (DDR) is essential to preserve genomic integrity and acts as a
29 barrier to cancer. The ATM pathway orchestrates the cellular response to DNA double strand
30 breaks (DSBs), and its attenuation is frequent during tumorigenesis. Here, we show that
31 NLRP3, a Pattern Recognition Receptor known for its role in the inflammasome complex
32 formation, interacts with the ATM kinase to control the early phase of DDR, independently of
33 its inflammasome activity. NLRP3 down-regulation in human bronchial epithelial cells
34 impairs ATM pathway activation as shown by an altered ATM substrate phosphorylation
35 profile, and due to impaired p53 activation, confers resistance to acute genomic stress.
36 Moreover, we found that NLRP3 is down-regulated in Non-Small Cell Lung Cancer
37 (NSCLC) tissues and NLRP3 expression is correlated with patient overall survival. NLRP3
38 re-expression in NSCLC cells restores appropriate ATM signaling. Our findings identify a
39 non-immune function for NLRP3 in genome integrity surveillance and strengthen the concept
40 of a functional link between innate immunity and DNA damage sensing pathways.

41

42

43 **INTRODUCTION**

44

45 Maintenance of genome integrity is crucial for cell survival. Toxic DNA double strand breaks
46 (DSBs) can arise from both exogenous sources, for instance exposure to ionizing radiation
47 (IR), or endogenous sources such as DNA replication stress. If they remain unrepaired or are
48 incorrectly repaired they represent a major risk factor for genome instability, a condition
49 known to favor tumorigenesis. One of the key proteins that orchestrates the rapid cellular

50 response to DSBs is the Ataxia-Telangiectasia Mutated (ATM) kinase. The early molecular
51 mechanism(s) leading to ATM activation upon DSB formation remain elusive. In resting
52 cells, ATM is present as an inactive dimer. Once recruited to DSBs via the action of the
53 MRE11-RAD50-NBS1 (MRN) complex, ATM autophosphorylates, monomerizes and
54 initiates a vast cascade of post-translational modifications that are essential for the DNA
55 Damage Response (DDR) ¹. Phosphorylation of the histone variant H2AX on Ser139
56 (γ H2AX) is one of the earliest events in the DDR and is crucial for an efficient recruitment of
57 DNA repair proteins to strand breaks to form Ionizing Radiation Induced Foci (IRIF) ²⁻⁵. The
58 scaffold protein MDC1 binds to γ H2AX and recruits more ATM to the DNA lesion thus
59 amplifying and maintaining the DNA damage signal ^{6,7}. ATM also phosphorylates many
60 downstream effector proteins including KAP1, p53 and CHK2, which induce effector
61 mechanisms such as the activation of cell cycle checkpoints, apoptosis or senescence ⁸. The
62 ATM pathway is tightly regulated and any dysregulation in these protection mechanisms
63 facilitates the progression of cells towards malignancy.

64 NLRP3 belongs to the Nod-Like Receptor (NLR) family, a family of cytosolic Pattern
65 Recognition Receptors (PRRs) involved in innate immunity ⁹. Upon sensing of Pathogen-
66 Associated Molecular Patterns (PAMPs) or Damage-Associated Molecular Patterns (DAMPs)
67 such as nigericin or ATP, respectively, NLRP3 triggers the assembly of a multi-protein
68 complex, the inflammasome, the function of which is to control caspase-1 activation ¹⁰⁻¹².
69 Activated caspase-1 induces the maturation of the pro-inflammatory cytokines IL-1 β and IL-
70 18, and eventually pyroptosis of the cell ^{13,14}. The NLRP3 inflammasome is mostly expressed
71 in macrophages and dendritic cells where its biological functions have been well
72 characterized. Whether NLRP3 exerts functions unrelated to immunity remains unknown ^{15,16}.
73 A previous study reported that in myeloid cells the NLRP3 inflammasome activity relies on
74 the presence of ATM, suggesting a functional link between these two pathways ¹⁷. Here, we

75 investigated whether NLRP3 controls the ATM pathway. We discovered that NLRP3 binding
76 to ATM is instrumental to early ATM activation and to trigger apoptosis in response to DNA
77 DSBs, and we report that NLRP3 expression is down-regulated in NSCLC.

78

79 **MATERIALS AND METHODS**

80 *Cell culture*

81 HBEC3-KT, HCC15, HCC366, HCC4017 and HCC461 were obtained from J. Minna, NCI-
82 H1703 (H1703), NCI-H292 (H292), NCI-H520 (H520), NCI-H661 (H661), NCI-H358
83 (H358), NCI-H1792 (H1792), NCI-H441 (H441) and SK-MES-1 from ATCC, and A549
84 from the PHE culture collection. HBEC3-KT cells were cultured in Keratinocyte-Serum Free
85 Medium (Invitrogen) supplemented with 12.5 mg of Bovine Pituitary Extract (Invitrogen) and
86 100 ng of epidermal growth factor (Invitrogen). H1792, A549, HCC15, HCC366, HCC4017,
87 HCC461 and H441 were cultured in RPMI medium, supplemented with 10% Fetal Bovine
88 Serum (FBS) and 1% penicillin/streptomycin, H1703, H292, H520, H358, H661 in RPMI,
89 10% FBS, 1 mM sodium pyruvate, 1 mM HEPES and 1% penicillin/streptomycin and SK-
90 MES-1 in RPMI, 10% FBS, 1 mM sodium pyruvate, 1 mM non-essential amino acids and 1
91 % penicillin/streptomycin (Invitrogen). *NLRP3* mutated cell lines are H661, H358, HCC15,
92 HCC366 and HCC4017. HeLa cells were cultured in DMEM 4.5 g/L of glucose, 10% FCS
93 and 1% penicillin/streptomycin. Treated cells received Etoposide (TEVA santé), HU (Sigma)
94 or γ -ray treatment 24 h post-transfection. For inflammasome activation, cells were primed
95 overnight with 10 μ g/mL poly(I:C) (Invivogen) and treated with nigericin (10 μ M, 6 h), or
96 ATP (5 mM, 30 min) (SIGMA). IL-1 β ELISA was purchased from BD. Z-VAD-fmk and z-
97 YVAD-fmk were from Enzo Life Science.

98

99 *Mice*

100 The NLRP3 flox mice were generated by the “clinique de la souris” Strasbourg. The exon 4
101 was flanked by 2 Lox-P sites in C57BL6 background. NLRP3^{flox/flox} mice were bred with
102 Rosa26-Cre-ERT2 mice. Bone marrow-derived macrophages were generated as previously
103 described³⁹ from +/+; Cre-ERT2 and Flox/Flox; Cre-ERT2 adult mice. To inactivate *Nlrp3*
104 (*Nlrp3*^{ΔΔ}), 4OHT (SIGMA) was added at the concentration of 0.5 μM from day 2 to day 7 of
105 differentiation in both genotypes for control. BMDM were treated with 100 μM Eto as
106 indicated.

107

108 *Cell transfection*

109 HBEC3-KT were seeded at 1.5x10⁵ cells per well in 6-well plates and were transfected with
110 non-targeting siRNA (SMART pool Non-targeting siRNA, Dharmacon) or NLRP3 siRNA
111 (SMARTpool, Dharmacon) using HiPerfect transfection reagent (Qiagen) or INTERFERin
112 (Polyplus transfection) following manufacturer’s instructions. HeLa cells were transfected
113 with Lipofetamin2000TM (Invitrogen). H292 cells were transfected using PEI method. Vectors
114 used pCR3-Flag-NLRP3 (FL, SHORT, PYD, NACHT, LRR), pcDNA3.1-Flag-His-ATM
115 (Addgene 31985), pcDNA3.1-mCherry-NLRP3. shRNA were from Genecopoeia,
116 hygromycin selection, *NLRP3*: forward: 5'-TAATACGACTCACTATAGGG-3' Reverse: 5'-
117 CTGGAATAGCTCAGAGGC-3'; control Forward: 5'-TAATACGACTCACTATAGGG-3'
118 Reverse: 5'-CTGGAATAGCTCAGAGGC-3'.

119 *Irradiation*

120 Cells were irradiated using a 6-MeV γ-ray clinical irradiator (SL 15 Phillips) at the Léon
121 Bérard Cancer Centre (Lyon, France) with a dose rate of 6 Gy.min⁻¹ to obtain the required
122 dose.

123

124 *ROS measurement*

125 For intracellular ROS staining, HBEC3-KT cells were incubated with 1 μ M of 2'-7'-
126 dichlorofluorescein diacetate (CM-H2DCFDA; Invitrogen) for 30 min at 37°C. For a positive
127 control, cells were pretreated with 5 μ M of ATM inhibitor (ATMi) (KU55933; Selleckchem)
128 for 5 h prior to staining. Stained cells were collected and analyzed on a BD FACSCalibur, and
129 data were analyzed using the FlowJo software.

130

131 *Mathematical modeling*

132 ATM dynamics was modeled using the following ordinary differential equation:

$$\frac{dA}{dt} = k_{IR} 1_{t \in [IR \text{ exposure}]} - k_{inact} A$$

133 where A is the concentration of activated ATM molecules (expressed in number of foci/cell),
134 k_{IR} is the activation rate (in number of foci/cell. h^{-1}), only present during irradiation, and
135 k_{inact} is the inactivation rate (in h^{-1}). A was set at zero at t_0 . This model assumed that ATM
136 molecules were in excess compared to the activated proportion.

137 The model is fitted to experimental data by estimating the optimal values for k_{IR} and k_{inact}
138 for each condition- siCTL or siNLRP3- using a weighted least-square approach⁴⁰. For
139 hypothesis A, i.e. NLRP3 enhances ATM activation, k_{IR} is assumed to be different for both
140 conditions whereas k_{inact} is taken identical. For hypothesis B, i.e. NLRP3 inhibits ATM
141 deactivation, k_{inact} is assumed to vary between siCTL and siNLRP3 conditions and k_{IR} is
142 assumed to remain identical. All computations were done in Matlab (Mathworks, USA).

143

144 *Generation of NLRP3 stably expressing cells*

145 The human *NLRP3* cDNA was inserted into the lentiviral vector pSLIKneo (addgene)
146 containing a TET-ON promoter using the Gateway recombination system (Invitrogen).

147 Sequences of the Gateway shuttle vectors are available upon request. Empty pSLIK vector
148 (without the ccdB containing Gateway recombination cassette) was produced by partial
149 digestion with Xba1 and Xho1 followed by religation. Viral particles were produced by
150 transfecting HEK293T cells with the lentiviral vectors and a second generation packaging
151 system. NCI-H292, NCI-H520 and A549 cells were either transduced with the empty pSLIK
152 control vector or the NLRP3 containing vector. NLRP3 expression was induced by adding 0.5
153 $\mu\text{g/mL}$ doxycycline (Takara Bio) to the cell culture medium.

154

155 *Western blotting*

156 Cells were washed with PBS and detached by trypsinization. Cell pellets were lysed in
157 Laemmli buffer x2 (Tris HCl 0.5 M pH 6.8; 0.5 M DTT; 0.5% SDS) and protein
158 concentrations were determined using the Bradford reagent (Biorad). Protein extracts were
159 separated on SDS-PAGE (8 % or 15 % or 4-15% gradient (vol/vol)) gels. Gels were
160 transferred onto nitrocellulose membranes (GE HealthCare and Biorad) for immunoblotting
161 with the following antibodies: anti-NLRP3 (Cryo-2, 1:1000) and anti-caspase-1 (Bally-1,
162 1:1000) from Adipogen, anti-ASC (1:2000) from ENZO Life Science, anti- γH2AX (JBW301,
163 1:1000), anti-P-Ser15-p53 (1:1000) and anti-ATM Ser1981 (10H11.E12, 1:200) were from
164 Millipore. Anti-P-KAP1Ser824 (1:1000), anti-KAP1 (1:1000) and anti-Nek7 (A302-684A)
165 from Bethyl Laboratories, anti-p53 (clone DO7 1:2000) and anti-NOXA (114C307, 1:1000)
166 from Santa Cruz, anti-ATM (#ab32420, 1/1000) from Abcam, anti-Flag (F7425 1/5000) from
167 Sigma, anti-XPO2 (GTX102005 1/1000) and anti-IPO5 (GTX114515 1/1000) from Genetex
168 and anti-actin (C4, 1:100,000) from MP Biomedical.

169 The Fiji and ImageLab programs were used for densitometric analysis of immunoblots, and
170 the quantified results were normalized as indicated in the figure legends.

171

172 *Cell fractionation*

173 HBEC3-KT were fractionated by adapting the method described by Hacot *et al.*⁴¹. The MgCl₂
174 concentration used for the hypotonic buffer was 0.75 mM. Equal amounts of proteins were
175 run by SDS-PAGE.

176

177 *Immunofluorescence*

178 Cells were plated onto sterile glass coverslips and fixed with PBS-PFA 4% (wt/vol) for 15
179 min at room temperature (RT) and washed twice in PBS. Cells were permeabilized with lysis
180 buffer (sucrose 300 mM, MgCl₂ 3 mM, Tris pH 7.0 20 mM, NaCl 50 mM, Triton X-100
181 0.5%) for 3-5 min at RT under slow agitation. The following antibodies were diluted in PBS-
182 BSA 4% and applied to the coverslips for 40 min at 37°C: anti-γH2AX (JBW301, 1:800), P-
183 ATM Ser1981 (10H11.E12, 1:200), and 53BP1 (1:500) from Millipore, and anti-MDC1
184 (1:200) from AbCam. For NLRP3 labeling, cells were fixed with PBS-PFA 4% (wt/vol) for
185 15 min at RT, washed twice in PBS and permeabilized with 1% triton X100. Anti-flag was
186 diluted in saturation buffer (PBS, 1% BSA; NaCl 0.02%; Tween 20 0.5%; SVF 3%) and
187 incubated on cells for 1 h. Cells were then incubated with Alexa-Fluor 488-conjugated anti-
188 mouse or Alexa-Fluor 555-conjugated anti-rabbit (1:800; Life Technologies) for 20 min at
189 37°C and in Hoechst (500 ng/mL in PBS) for 10 min at RT. Fluorescence microscopy
190 pictures were taken using a Nikon Eclipse Ni-E microscope, and confocal Zeiss LSM 780.
191 The Fiji program was used to analyze fluorescence intensity.

192

193 *Live imaging*

194 mCherry-NLRP3 transfected H292 were imaged using a confocal spinning disk inverted
195 microscope (Leica, Yokogawa). Vital Hoechst was used at 0.5 μg/mL. The Fiji program was
196 used to analyze fluorescence intensity.

197

198 *Co-immunoprecipitation*

199 HeLa cells were transfected using Lipofectamin2000TM (Invitrogen) according to
200 manufacturer's protocol, and lyzed in the following buffer: Tris HCl 100 mM pH 8.0, 10 mM
201 MgCl₂, 90 mM NaCl, 0.1% Triton X-100, Complete® tablet (Roche). Immunoprecipitation
202 was performed using M2-agarose beads (A2220 Sigma) overnight at 4°C.

203

204 *Proximity Ligation Assay*

205 HBECT3-KT and HeLa cells were seeded onto glass coverslips and processed as described by
206 the manufacturer's protocol (Duolink® PLA Technology, Sigma). Antibodies used NLRP3
207 1/500 (ABF23, Millipore), ATM 1/500 (2C1, Abcam). Quantification was carried out using
208 the macro published by Poulard *et al* ⁴².

209

210 *IL-1β Luminex Assay*

211 IL-1β levels in cell supernatants were analyzed using the Magnetic Luminex Screening Assay
212 according to the manufacturer's protocol (R&D Systems). The samples were read using the
213 Bioplex-200 from BioRad.

214

215 *Quantitative reverse transcription PCR*

216 Cells were washed and detached by trypsinization. RNA was extracted using NucleoSpin®
217 RNA kit (Macherey Nagel). Five hundred nanograms to one microgram of RNA were reverse
218 transcribed using SuperScript II reverse transcriptase and oligo(dT) primers (Life
219 technologies) and RNAsin (Promega). cDNAs were quantified by real-time PCR using a
220 SYBR® Green PCR Master Mix (Applied Biosystems) on a ABI Prism® 7000 (Applied
221 Biosystems) or CFX Connect Real-Time system (BioRad). Sequences of the primers NLRP3

222 Forward 5'-GAAGAAAGATTACCGTAAGAAGTACAGAAA; Reverse 5'-
223 CGTTTGTTGAGGCTCACACTCT; ESD 5'-TTAGATGGACAGTTAC TCCCTGATAA;
224 Reverse 5'-GGTTGCAATGAAGTAGTAGCTATGAT; HPRT1 Forward 5'-
225 CATTATGCTGAGGATTTGGAAAGG; Reverse 5'-TGTAGCCCTCTGTGTGCTCAAG;
226 CBP Forward 5'-CGGCTGTTTAACTTCGCTTC; Reverse 5'-
227 CACACGCCAAGAAACAGTGA. NOXA Forward 5'-GGAGATGCCTGGGAAGAAG;
228 Reverse 5'-CCTGAGTTGAGTAGCACACTCG; PUMA Forward 5'-
229 CCTGGAGGGTCCTGTACAATCTCAT; Reverse 5'-
230 GTATGCTACATGGTGCAGAGAAAG; ACTIN Forward 5'-
231 AGCACTGTGTTGGCGTACAG; Reverse 5'-TCCCTGGAGAAGAGCTACGA.

232 NLRP3 mRNA amounts in different NSCLC cell lines were normalized against *ESD* (Fig.
233 1B) or in human samples on *CPB* and *HPRT1* (Fig. 1D) mRNA levels or in HBEC-KT on
234 *HPRT1* (Fig. 5C).

235

236 *Caspase-3/7 assay*

237 Cells were cultured in 96-well plates and treated with 50 μ M of Etoposide for 12 h or with
238 200 ng/mL Trail (Peprotech) and 1 mM MG132 (Sigma). Caspase 3/7 activity was assessed
239 using the Caspase-Glo 3/7 assay reagent (Promega) following the manufacturer's instructions.
240 The luminescence was measured using a TECAN Infinite M200PRO luminometer microplate
241 reader. To normalize the results, a second plate was stained with crystal violet and analyzed
242 as described in the *crystal violet cytotoxicity assay* below.

243

244 *Crystal Violet cytotoxicity assay*

245 Cells were stained with 0.5% crystal violet (Sigma-Aldrich Corp.) in 30% methanol for 20
246 minutes at room temperature. Cells were lysed in a 1% SDS (Sigma-Aldrich Corp.) solution.

247 The absorbance of the solution was measured using a TECAN Infinite M200PRO microplate
248 reader at a wavelength of 595 nm.

249

250 *Tissues from NSCLC patients*

251 Frozen lung tumor tissues from non-treated patients were obtained from the Biological
252 Resource Centre in Grenoble (Centre de Ressources biologiques de Grenoble) n°BB-0033-
253 00069 and in accordance with the ethical laws. RNA was extracted from regions containing
254 mainly malignant cells using Allprep RNA/DNA kit from Qiagen.

255

256 *TCGA data analysis*

257 RNAseqV2 data of lung adenocarcinoma (LUAD) and corresponding clinical data were
258 downloaded from The Cancer Genome Atlas TCGA data portal. Cox regression model was
259 used to estimate hazard ratio (HR) and 95% confidence intervals (CIs) for overall survival
260 (OS) and progression-free interval (PFI). Survival curve was estimated by the Kaplan–Meier
261 method. Optimal cutoff for NLRP3 expression was chosen based on a maximally selected
262 rank statistic⁴³.

263

264 *Statistical analysis*

265 Statistical analysis of the experimental data was performed using Graphpad. Unpaired group
266 comparisons were done using two-tailed Student t-test for most figures, Mann-Whitney test
267 for Figure 5A and B and multiple comparisons for two-way ANOVA for Figure 5C.

268

269 **RESULTS**

270 **Loss of NLRP3 impairs γ H2AX and P-ATM IRIF formation.**

271 To identify novel NLRP3 functions potentially linked to the regulation of the ATM pathway,
272 we exposed HBEC3-KT cells to IR (2 Gy) and assessed the activation of the DDR pathway in
273 the presence or absence of NLRP3. In control cells, the number of nuclear γ H2AX (Ser139)
274 IRIF peaked around 1 h after IR treatment and then decreased with time as the cells
275 underwent DNA repair (Fig. 1A and Suppl. Fig. 1A). In contrast, in the absence of NLRP3 a
276 significantly lower number of γ H2AX IRIF were initially formed, and detected at all
277 subsequent time points. This difference was greatest 1 h post IR and persisted over the time
278 course of the study. ATM activation by DSBs relies on its monomerization which coincides
279 with autophosphorylation on Ser1981¹. Using the presence of P-ATM(Ser1981) IRIF as an
280 endpoint for ATM activation we observed as early as 15 min post IR, fewer P-ATM foci in
281 the absence of NLRP3, and the difference remained significant at 1 h and 5 h post-irradiation
282 (Fig. 1B). Next, we tested whether the positive amplification loop required for optimal ATM
283 activation was altered in the absence of NLRP3 by assessing the recruitment of MDC1 to
284 DSBs. In siNLRP3-treated cells a decreased number of MDC1 foci were found compared
285 with siCTL-treated cells, clearly illustrating a defect in the recruitment of MDC1 to DSBs,
286 and, as a consequence, a defect in the ability to fully activate ATM (Fig. 1C and Suppl. Fig.
287 1B). 53BP1 is a DNA repair protein that also forms IRIF in response to DSBs but in an ATM-
288 independent manner¹⁸. The levels of 53BP1 foci were similar in the absence or presence of
289 NLRP3 (Fig. 1D and Suppl. Fig. 1C), leading us to conclude that the decrease in the ability to
290 form γ H2AX and P-ATM foci supports a role for NLRP3 in the radiation-induced ATM DSB
291 signaling pathway. This hypothesis was further investigated using mechanistic mathematical
292 modeling (see Methods). Based on our experimental findings that NLRP3 KD reduced the
293 observed number of P-ATM molecules recruited at DSBs, two hypotheses were investigated:
294 A) NLRP3 enhances ATM activation, B) NLRP3 inhibits ATM deactivation (Suppl. Fig. 1D).
295 Hypothesis A achieved a nearly perfect fit to data whereas hypothesis B was not able to

296 reproduce the correct dynamics (SSR_A=0.052, SSR_B=0.29, Figure 1E). The model allowed
297 to predict that the ATM activation rate in siNLRP3 conditions k_{IR} was nearly half of that in
298 siCTL cells as the ratio $\frac{k_{IR}^{control}}{k_{IR}^{NLRP3}}$ was equal to 1.66. Thus, the model A, which best
299 recapitulated our data, supports the notion that NLRP3 enhances ATM activation.

300

301 **NLRP3 is required for optimal ATM activation.**

302 To determine whether NLRP3 played a broader role in the activation of the ATM pathway,
303 we examined the phosphorylation of ATM downstream effectors that regulate cellular
304 outcome in response to different DSB inducers. First, we showed that the absence of NLRP3
305 resulted in lower levels of KAP1 Ser824 phosphorylation in response to IR (Fig. 2A). Second,
306 we tested the response of HBEC3-KT cells to two chemotherapeutic agents known to induce
307 DSBs, etoposide (Eto), a topoisomerase II inhibitor, and hydroxyurea (HU), that depletes
308 cellular dNTP pools, initially inducing stalled replication forks and, following longer
309 exposure times, fork collapse and DSBs¹⁹. Similarly, the absence of NLRP3 led to lower
310 phosphorylation levels of KAP1 and p53 2 h to 6 h post-treatment with etoposide (Fig. 2B
311 and C) or HU treatment (Suppl. Fig. 2A). NLRP3 down-regulation also resulted in decreased
312 P-ATM irrespective of Eto concentrations (Suppl. Fig. 2B and C), and decreased γ H2AX foci
313 formation upon Eto treatment (Suppl. Fig. 2D). These results suggest that ATM is defective in
314 the absence of NLRP3. Previous studies reported that ATM dysfunction induces ROS
315 production in cells^{17,20}. Consistent with these studies NLRP3-depleted cells displayed
316 enhanced ROS content compared to control cells, which did not increase further by the
317 addition of the ATM inhibitor KU55933 (Suppl Fig. 2E). Collectively, these results strongly
318 support the notion that NLRP3 is required for optimal ATM activation in response to DSBs.

319 We then wondered whether NLRP3 was globally required for ATM activation using a
320 heterologous model. Murine bone marrow-derived macrophages (BMDMs) either WT or

321 NLRP3^{Δ/Δ} treated with Eto displayed deficient ATM activation, as evidenced by reduced
322 ATM and KAP1 phosphorylation compared to controls (Fig. 2D). As we found A549 and
323 H292 lung cancer cells did not express NLRP3, we re-expressed NLRP3 using a doxycycline-
324 inducible system in these NSCLC tumor cell lines, and evaluated ATM activation after IR
325 exposure by assessing the number of P-ATM and γ H2AX IRIF. NLRP3 re-expression
326 increased the levels of H2AX and ATM activating phosphorylations in both cell lines 1 h
327 post-treatment (Fig. 3 A to D and Suppl. Fig. 3A to D). In addition, upon Eto treatment, the
328 phosphorylation kinetics of the downstream effectors p53 and KAP1 in H292 re-expressing
329 NLRP3 resembled those observed in non-tumoral control cells (Fig. 3E). Similar results were
330 obtained in H520 IR-treated cells reconstituted with NLRP3 (Suppl. Fig. 3E). Thus, NLRP3
331 re-expression improved ATM activation.

332

333 **NLRP3 controls the ATM pathway independently of its inflammasome activity.**

334 To assess if this new role for NLRP3 in DNA damage signaling is dependent on its well-
335 known inflammasome function, caspase-1 was knocked down using siRNA. The loss of
336 caspase-1 did not alter the level of γ H2AX after Eto treatment (Fig. 4A). In addition, no
337 significant difference in the phosphorylation of H2AX was observed in HBEC3-KT cells
338 treated with the pan-caspase inhibitor z-VAD-fmk or the caspase-1 inhibitor z-YVAD-fmk
339 prior to HU exposure. These results would suggest that neither caspase-1 nor another caspase
340 activity was involved in the activation of the ATM pathway, thus excluding apoptosis as a
341 source of H2AX phosphorylation (Fig. 4B). In addition, DNA damage did not activate the
342 inflammasome as IL-1 β release was barely detectable in cell supernatants after HU or IR
343 treatments, nor could we detect cleaved caspase-1 after Eto treatment (Fig. 4C, D, and E).
344 Thus, DNA DSBs do not activate the catalytic activity of the inflammasome.

345

346 **NLRP3 forms a complex with ATM.**

347 To determine how NLRP3 regulates ATM activity, we tested whether these two proteins
348 could interact with each other. In HeLa cells, that do not express endogenous NLRP3, co-
349 immunoprecipitation of Flag-ATM pulled down mCherry-NLRP3 (Fig. 5A). Moreover,
350 Flag-NLRP3 co-immunoprecipitated endogenous ATM (Fig. 5B)²¹. Eto treatment dissociated
351 the interaction, suggesting that ATM and NLRP3 formed a complex under basal cell
352 condition (Fig. 5B). We then mapped the NLRP3 domain involved in its binding to ATM. We
353 showed that ATM interacted with the NACHT (domain present in neuronal apoptosis
354 inhibitor protein, the major histocompatibility complex class II transactivator, HET-E and
355 TPI), and the LRR (Leucin Rich Repeats) domains but not with the PYD (Pyrin) domain,
356 which is known to mediate homotypic interactions involved in inflammasome formation (Fig.
357 5C)¹⁰. NEK7 was used as a positive assay control, as it is a known partner of NLRP3 (Fig.
358 5C). We next investigated whether NLRP3 was able to translocate to the nucleus. Cell
359 fractionation experiments revealed that endogenous NLRP3 was present in both the cytosolic
360 and nuclear fractions (Suppl. Fig. 4A) supporting earlier findings²². Interestingly, IF labeling
361 of NLRP3 domains revealed nuclear localizations for the NACHT and the LRR domains, and
362 a cytosolic localization for the PYD domain, which self-oligomerized as previously described
363 for ASC PYD (Suppl. Fig. 4B)²³. Using this technique, short and full length (FL) NLRP3
364 were weakly detected in the nucleus (Suppl. Fig. 4B). However, live-imaging of mCherry-
365 NLRP3 revealed its presence in the cell nucleus (Suppl. Fig. 4C). Consistently, co-
366 immunoprecipitation experiments revealed that NLRP3 bound to IPO5 and XPO2 two
367 proteins involved in nuclear import and export, respectively, which we identified by mass
368 spectrometry (Fig. 5C)^{24,25}.

369 Using Proximity Ligation Assay (PLA), we also showed in HeLa cells that Flag-NLRP3 and
370 endogenous ATM formed a complex (Suppl. Fig. 4D). Importantly, we validated that

371 endogenous ATM and NLRP3 interacted in HBEC3-KT cells, and that the complex was
372 dissociated upon Eto treatment (Fig. 5D). We also observed after DNA damage that a smaller
373 fraction of ATM was detected by IF in the nucleus of NLRP3-depleted cells compared with
374 control cells (Suppl. Fig. 5A, B). Collectively, these results establish that under homeostatic
375 conditions NLRP3 forms a complex with ATM, which dissociates upon DSB formation.

376

377 **NLRP3-depleted cells are resistant to genotoxic stress-induced cell death.**

378 Because ATM activity controls cell fate decisions in response to genotoxic stress, we next
379 monitored cell death in response to Eto treatment. In NLRP3-depleted HBEC3-KT cells, less
380 caspase-3/7 activity was detected compared with control conditions, and an increase in the
381 number of viable cells was observed (Fig. 6A and B). These results suggest that decreased
382 NLRP3 expression protects cells from etoposide-induced apoptosis. Indeed, the induction of
383 *PUMA* and *NOXA/PMAIP1*, two p53 apoptosis effector genes, was significantly reduced in
384 the absence of NLRP3 compared to control cells (Fig. 6C and D)^{26,27}. This response was
385 specific to genotoxic stress as the induction of apoptosis via death receptor activation using a
386 combination of TRAIL and MG132 did not result in impaired apoptosis in cells depleted for
387 NLRP3 (Suppl. Fig. 6A and B).

388

389 **NLRP3 is down-regulated in NSCLC.**

390 GWAS studies reported that *NLRP3* is frequently mutated in NSCLC, but we found that A549
391 and H292 cells, isolated from NSCLC patients, do not express NLRP3. To extend this
392 observation, we assembled a panel of NSCLC cell lines, and included 3 HBEC3-KT cell lines
393 for comparison²⁸. Paradoxically, in most of the NSCLC cell lines, including cell lines
394 reported to carry NLRP3 mutations, the NLRP3 protein was barely detectable (Fig. 7A and
395 Suppl. Fig. 7A), and very low levels of *NLRP3* mRNA were observed by Q-RT-PCR in

396 comparison with HBEC3-KT cells (Fig. 7B). Among the 3 HBEC3-KT lines, the HBEC3-ET
397 cells did not express NLRP3, and those cells displayed properties of malignant transformation
398 since they were able to grow in an anchorage-independent manner (Suppl Fig. 7B). These
399 results suggest that NLRP3 expression is down-regulated in malignant cells. To validate these
400 observations, we obtained a set of RNA samples from a cohort of patients with primary
401 NSCLC and from adjacent normal lung tissues. As shown in Fig. 7C, *NLRP3* mRNA was
402 detectable in normal lung tissues, while it was significantly down-regulated in NSCLC
403 tissues. Finally, analysis of TCGA data showed that low NLRP3 expression in lung
404 adenocarcinoma (LUAD) was associated with better overall survival and better progression-
405 free interval (Fig. 7D and E). Altogether, these results suggest a down-regulation of NLRP3
406 in NSCLC, and a positive correlation in LUAD between NLRP3 levels and patient outcome.

407

408 **Discussion**

409 Functional links between innate immunity and DNA damage sensing pathways have been
410 described. For instance, ATM was recently shown to be required in macrophages for optimal
411 NLRP3 and NLRC4 inflammasome functions because its inactivation altered the ROS
412 balance and therefore impaired inflammasome assembly¹⁷. It was also suggested that DDR
413 proteins such as RAD50 or BRCA1 are involved in the sensing of nucleic acids from viral
414 pathogens in the cytosol^{29,30}. However, little is known about the contribution of PRRs to the
415 sensing of stress like DNA damage. Here, we demonstrate that NLRP3 is crucial to reach
416 optimal ATM activation. Under homeostatic conditions, our PLA data showed that NLRP3
417 forms a complex with ATM in the cytosol, suggesting that NLRP3 binds to the inactive ATM
418 dimer. ATM has already been reported to be found in the cell cytosol^{20,31}. Upon DNA DSB
419 formation, the complex dissociates to allow ATM relocalization and monomerization onto
420 DNA breaks. In the absence of NLRP3, decreased levels of P-ATMSer1981 foci were

421 observed herein, together with a decreased nuclear ATM pool. These observations suggest
422 that NLRP3 may control either ATM translocation to the nucleus or ATM monomerization.
423 Consequently, the formation of γ H2AX and MDC1 IRIF, which are both essential for the
424 positive ATM amplification loop signaling, were also impaired in NLRP3 KD cells⁶. This led
425 to a less active ATM as illustrated by the reduced phosphorylation of its substrates KAP-1
426 and p53, and, importantly, cells became more resistant to apoptosis.

427 No caspase-1 activation and no significant IL-1 β production was detected upon DNA DSB
428 induction. Our findings contrast with those of R. Flavell's group, who demonstrated in mouse
429 models that the severe damage caused to the gastrointestinal tract and the hematopoietic
430 system in response to whole body γ -irradiation are due to the activation of the AIM2
431 inflammasome by DSBs, which cause massive cell death by caspase-1-dependent pyroptosis
432 in these fast renewing tissues. These observations would suggest that tissue and species-
433 specific differences may exist that clearly warrant further investigation³².

434 Using different approaches which included restoring NLRP3 expression in NSCLC cell lines
435 displaying low levels of inflammasome proteins, we identified a novel non-inflammasome
436 function for NLRP3 in the DNA damage pathway. This previously unappreciated role for
437 NLRP3 in the ATM pathway may be due to the fact that many common cellular models used
438 in laboratories do not express NLRP3 (e.g. MEF, HeLa, 293, A549). Altogether, our results
439 highlight that NLRP3 is not only a major player in innate immunity but is also a key factor
440 involved in the preservation of genome integrity through the modulation of the ATM
441 signaling pathway in response to DSBs.

442 The DDR is known to be a barrier to cancer in the early phases of tumorigenesis^{33,34}. *TP53* is
443 frequently mutated in cancer, and the ATM pathway is down-regulated in many solid tumors:
444 11% of NSCLC carry somatic mutations in *ATM* and 41% of lung adenocarcinoma have
445 reduced ATM protein expression³⁵⁻³⁸. Although, several cancer genomic studies have

446 reported that *NLRP3* is frequently mutated in NSCLC, our data actually suggest that in
447 NSCLC primary human tissues and cell lines its expression is significantly lower compared to
448 normal tissue. This down-regulation of *NLRP3* expression during malignant transformation
449 may represent an additional mechanism to attenuate ATM and p53 signaling pathways,
450 allowing cells to survive genotoxic stress, despite the presence of genome alterations. Thus,
451 the loss of *NLRP3*, and the subsequent impairment of the ATM pathway could be an event
452 allowing cells to progress towards malignancy.

453

454 **Acknowledgements:** We thank John Minna for sharing the HBEC3-KT and NSCLC cells, Dr
455 Foray's team and Marine Malfroy for technical help and Agnès Tissier and Pascale Bertrand
456 for helpful discussions. We thank Christophe Vanbelle and Christophe Chamot for their
457 assistance on confocal microscope image acquisition. M.B. was supported by the ANRT, V.P.
458 by the plan Cancer, Ligue Contre le Cancer Comité de l'Ain, the ARC foundation, and the
459 Fondation pour la Recherche Médicale DEQ20170336744, A.L.H. by the ARC foundation
460 and a Marie Skodolvska-Curie grant, N.G. was supported by the CLARA, and B.G. by the
461 ARC foundation. B.P. was supported by the ERC.

462

463 **Author contributions:** M.B.W., A.L.H., J.G., S.H., J.H. and V.P. designed and analyzed
464 experiments. M.B.W., A.L.H., J.G., B.G., S.H., Y.C., L.G. and V.P. performed experiments.
465 F.G., B.B., B.P., S.L., B.P. and N.G. provided reagents. M.B.W., A.L.H., J.G., S.H., J.H. and
466 V.P. contributed to the manuscript writing and figure constructions.

467

468 **Competing interests:** the authors declare no financial competing interest.

469

470

471 **REFERENCES**

- 472 1 Bakkenist CJ, Kastan MB. DNA damage activates ATM through intermolecular
473 autophosphorylation and dimer dissociation. *Nature* 2003; **421**: 499–506.
- 474 2 Celeste A, Petersen S, Romanienko PJ, Fernandez-Capetillo O, Chen HT, Sedelnikova
475 O a *et al.* Genomic instability in mice lacking histone H2AX. *Science* 2002; **296**: 922–
476 927.
- 477 3 Xie A, Puget N, Shim I, Odate S, Jarzyna I, Bassing CH *et al.* Control of sister
478 chromatid recombination by histone H2AX. *Mol Cell* 2004; **16**: 1017–25.
- 479 4 Burma S, Chen BP, Murphy M, Kurimasa A, Chen DJ. ATM phosphorylates histone
480 H2AX in response to DNA double-strand breaks. *J Biol Chem* 2001.
481 doi:10.1074/jbc.C100466200.
- 482 5 Paull TT, Rogakou EP, Yamazaki V, Kirchgessner CU, Gellert M, Bonner WM. A
483 critical role for histone H2AX in recruitment of repair factors to nuclear foci after DNA
484 damage. *Curr Biol* 2000; **10**: 886–895.
- 485 6 Lou Z, Minter-Dykhouse K, Franco S, Gostissa M, Rivera MA, Celeste A *et al.* MDC1
486 maintains genomic stability by participating in the amplification of ATM-dependent
487 DNA damage signals. *Mol Cell* 2006; **21**: 187–200.
- 488 7 Stucki M, Clapperton J a., Mohammad D, Yaffe MB, Smerdon SJ, Jackson SP. MDC1
489 Directly Binds Phosphorylated Histone H2AX to Regulate Cellular Responses to DNA
490 Double-Strand Breaks. *Cell* 2005; **123**: 1213–1226.
- 491 8 Smith J, Tho LM, Xu N, Gillespie DA. The ATM-Chk2 and ATR-Chk1 pathways in
492 DNA damage signaling and cancer. *Adv Cancer Res* 2010; **108**: 73–112.
- 493 9 Martinon F, Tschopp J. NLRs join TLRs as innate sensors of pathogens. *Trends*
494 *Immunol* 2005; **26**: 447–454.

- 495 10 Schroder K, Tschopp J. The inflammasomes. *Cell* 2010; **140**: 821–32.
- 496 11 Mariathasan S, Weiss DS, Newton K, McBride J, O'Rourke K, Roose-Girma M *et al.*
497 Cryopyrin activates the inflammasome in response to toxins and ATP. *Nature* 2006;
498 **440**: 228–32.
- 499 12 Pétrilli V, Dostert C, Muruve D a DA, Tschopp J, Petrilli V, Dostert C *et al.* The
500 inflammasome: a danger sensing complex triggering innate immunity. *Curr Opin*
501 *Immunol* 2007; **19**: 615–22.
- 502 13 Agostini L, Martinon F, Burns K, McDermott MF, Hawkins PN, Tschopp J. NALP3
503 forms an IL-1beta-processing inflammasome with increased activity in Muckle-Wells
504 autoinflammatory disorder. *Immunity* 2004; **20**: 319–325.
- 505 14 Mariathasan S, Monack DM. Inflammasome adaptors and sensors: intracellular
506 regulators of infection and inflammation. *Nat Rev Immunol* 2007; **7**: 31–40.
- 507 15 Guarda G, Zenger M, Yazdi AS, Schroder K, Ferrero I, Menu P *et al.* Differential
508 expression of NLRP3 among hematopoietic cells. *J Immunol* 2011; **186**: 2529–2534.
- 509 16 Wang W, Wang X, Chun J, Vilaysane A, Clark S, French G *et al.* Inflammasome-
510 Independent NLRP3 Augments TGF- β Signaling in Kidney Epithelium. *J Immunol*
511 2013; **190**: 1239–49.
- 512 17 Erttmann SF, Härtlova A, Sloniecka M, Raffi FAM, Hosseinzadeh A, Edgren T *et al.*
513 Loss of the DNA Damage Repair Kinase ATM Impairs Inflammasome-Dependent
514 Anti-Bacterial Innate Immunity. *Immunity* 2016; **45**: 106–118.
- 515 18 DiTullio RA, Mochan TA, Venere M, Bartkova J, Sehested M, Bartek J *et al.* 53BP1
516 functions in an ATM-dependent checkpoint pathway that is constitutively activated in
517 human cancer. *Nat Cell Biol* 2002; **4**: 998–1002.
- 518 19 Saintigny Y, Delacôte F, Varès G, Petitot F, Lambert S, Averbek D *et al.*

- 519 Characterization of homologous recombination induced by replication inhibition in
520 mammalian cells. *EMBO J* 2001; **20**: 3861–3870.
- 521 20 Alexander A, Cai S-L, Kim J, Nanez A, Sahin M, MacLean KH *et al.* ATM signals to
522 TSC2 in the cytoplasm to regulate mTORC1 in response to ROS. *Proc Natl Acad Sci U*
523 *S A* 2010; **107**: 4153–8.
- 524 21 Shi H, Wang Y, Li X, Zhan X, Tang M, Fina M *et al.* NLRP3 activation and mitosis
525 are mutually exclusive events coordinated by NEK7, a new inflammasome component.
526 *Nat Immunol* 2015; **advance on**. doi:10.1038/ni.3333.
- 527 22 Bruchard M, Rebé C, Derangère V, Togbé D, Ryffel B, Boidot R *et al.* The receptor
528 NLRP3 is a transcriptional regulator of TH2 differentiation. *Nat Immunol* 2015; **16**:
529 859–70.
- 530 23 Lu A, Magupalli VG, Ruan J, Yin Q, Atianand MK, Vos MR *et al.* Unified
531 polymerization mechanism for the assembly of asc-dependent inflammasomes. *Cell*
532 2014; **156**: 1193–1206.
- 533 24 Soniat M, Chook YM. Nuclear localization signals for four distinct karyopherin- β
534 nuclear import systems. *Biochem J* 2015; **468**: 353–362.
- 535 25 Güttler T, Görlich D. Ran-dependent nuclear export mediators: a structural perspective.
536 *EMBO J* 2011; **30**: 3457–3474.
- 537 26 Shibue T, Takeda K, Oda E, Tanaka H, Murasawa H, Takaoka A *et al.* Integral role of
538 Noxa in p53-mediated apoptotic response. *Genes Dev* 2003. doi:10.1101/gad.1103603.
- 539 27 Nakano K, Vousden KH. PUMA, a novel proapoptotic gene, is induced by p53. *Mol*
540 *Cell* 2001. doi:10.1016/S1097-2765(01)00214-3.
- 541 28 Ramirez RD, Sheridan S, Girard L, Sato M, Kim Y, Pollack J *et al.* immortalization of
542 human bronchial epithelial cells in the absence of viral oncoproteins. *Cancer Res* 2004;

- 543 **64**: 9027–34.
- 544 29 Roth S, Rottach A, Lotz-Havla AS, Laux V, Muschaweckh A, Gersting SW *et al.*
545 Rad50-CARD9 interactions link cytosolic DNA sensing to IL-1 β production. *Nat*
546 *Immunol* 2014; **15**: 538–45.
- 547 30 Dutta D, Dutta S, Veettil MV, Roy A, Ansari MA, Iqbal J *et al.* BRCA1 Regulates
548 IFI16 Mediated Nuclear Innate Sensing of Herpes Viral DNA and Subsequent
549 Induction of the Innate Inflammasome and Interferon- β Responses. *PLoS Pathog* 2015;
550 **11**: e1005030.
- 551 31 Fiévet A, Bellanger D, Rieunier G, Dubois d’Enghien C, Sophie J, Calvas P *et al.*
552 Functional classification of ATM variants in ataxia-telangiectasia patients. *Hum Mutat*
553 2019. doi:10.1002/humu.23778.
- 554 32 Hu S, Peng L, Kwak Y-TT, Tekippe EM, Pasare C, Malter JS *et al.* The DNA Sensor
555 AIM2 Maintains Intestinal Homeostasis via Regulation of Epithelial Antimicrobial
556 Host Defense. *Cell Rep.* 2015; **13**: 1922–36.
- 557 33 Bartkova J, Horejsí Z, Koed K, Krämer A, Tort F, Zieger K *et al.* DNA damage
558 response as a candidate anti-cancer barrier in early human tumorigenesis. *Nature* 2005;
559 **434**: 864–870.
- 560 34 Lantuejoul S, Raynaud C, Salameire D, Gazzeri S, Moro-Sibilot D, Soria J-C *et al.*
561 Telomere maintenance and DNA damage responses during lung carcinogenesis. *Clin*
562 *Cancer Res* 2010; **16**: 2979–88.
- 563 35 Ding L, Getz G, Wheeler DA, Mardis ER, McLellan MD, Cibulskis K *et al.* Somatic
564 mutations affect key pathways in lung adenocarcinoma. *Nature* 2008; **455**: 1069–1075.
- 565 36 Hammerman PS, Hayes DN, Wilkerson MD, Schultz N, Bose R, Chu AALA *et al.*
566 Comprehensive genomic characterization of squamous cell lung cancers. *Nature* 2012;

- 567 **489**: 519–25.
- 568 37 Imielinski M, Berger AH, Hammerman PS, Hernandez B, Pugh TJ, Hodis E *et al.*
569 Mapping the hallmarks of lung adenocarcinoma with massively parallel sequencing.
570 *Cell* 2012; **150**: 1107–1120.
- 571 38 Villaruz LC, Jones H, Dacic S, Abberbock S, Kurland BF, Stabile LP *et al.* ATM
572 protein is deficient in over 40% of lung adenocarcinomas. *Oncotarget* 2016.
573 doi:10.18632/oncotarget.9757.
- 574 39 Guey B, Bodnar M, Manié SNSN, Tardivel A, Petrilli V. Caspase-1 autoproteolysis is
575 differentially required for NLRP1b and NLRP3 inflammasome function. *Proc Natl*
576 *Acad Sci U S A* 2014; **111**: 17254–9.
- 577 40 Hill RJW, Innominato PF, Lévi F, Ballesta A. Optimizing circadian drug infusion
578 schedules towards personalized cancer chronotherapy. *PLOS Comput Biol* 2020; **16**:
579 e1007218.
- 580 41 Hacot S, Coute Y, Belin S, Albaret MA, Mertani HC, Sanchez J-C *et al.* Isolation of
581 nucleoli. *Curr Protoc Cell Biol* 2010; **Chapter 3**: Unit3.36.
- 582 42 Poulard C, Jacquemetton J, Pham TH, Le Romancer M. Using proximity ligation assay
583 to detect protein arginine methylation. *Methods* 2019.
584 doi:10.1016/J.YMETH.2019.09.007.
- 585 43 Lausen B, Schumacher M. Maximally Selected Rank Statistics. *Biometrics* 1992; **48**:
586 73–85.
- 587
- 588
- 589

590

591 **FIGURE LEGENDS**

592 **Figure 1.** NLRP3 down-regulation impairs ATM-dependent IRIF formation and DNA
593 damage signaling in response to DNA double strand breaks.

594 (A to D) HBEC3-KT transfected with control (siCTL) or NLRP3 siRNA (siNLRP3) were
595 treated with IR (2 Gy). The number of nuclear γ H2AX (A), MDC1 (B), P-ATM (C), and
596 53BP1 (D) IRIF were determined by immunofluorescence at indicated time points. IF of the 1
597 h time point is shown (x60). Hoechst (blue) was used to stain nuclei. Representative of four
598 (A, C) and two independent experiments (B, D) ($64 \leq n \leq 148$) Scale bars 10 μ m. (E)
599 Mathematical modeling of ATM and NLRP3 interactions. Two hypotheses were investigated
600 A) NLRP3 enhances ATM activation, B) NLRP3 inhibits ATM deactivation.

601

602 **Figure 2.** NLRP3 is instrumental for optimal ATM activation.

603 (A) HBEC3-KT transfected with indicated siRNA were IR treated (10 Gy) and collected at
604 different time points and P-KAP1 analyzed by immunoblotting. (B) HBEC3-KT control
605 siRNA and NLRP3 siRNA were exposed to Eto (100 μ M) for indicated time points and P-
606 KAP1 and P-p53 were analyzed by immunoblot. (C) Relative quantification of immunoblot
607 of 3 independent experiments as shown in (D). (E) Bone marrow-derived macrophages of
608 wild type NLRP3 or NLRP3-depleted mice were treated with Eto 100 μ M over time and P-
609 ATM and P-KAP1 were analyzed by immunoblotting (representative of 2 experiments). Data
610 represent mean \pm SEM, *** $P < 0.001$, **** $P < 0.0001$, ns: not significant (unpaired t-test).

611

612 **Figure 3.** Expression of NLRP3 in NSCLC cell lines improves ATM activation after the
613 induction of DNA DSBs.

614 A549 (**A** and **B**) or H292 (**C** and **D**) cells stably expressing a doxycycline-inducible NLRP3
615 lentiviral vector (pSLIK NLRP3) induced or not with 0.5 $\mu\text{g}/\text{mL}$ doxycycline were irradiated
616 with 2 Gy and P-ATM (**A** and **C**) and γH2AX (**B** and **D**) IRIF assessed 1 h post-treatment. (**E**)
617 H292 cells stably expressing the control or NLRP3 lentiviral vector were induced with
618 doxycycline 24 h before being treated with etoposide over a time course of 16 h. KAP1 and
619 p53 phosphorylation was analyzed by immunoblot at the indicated time points. One
620 representative experiment out of 3. **** $P < 0.0001$, *** $P < 0.001$, * $P < 0.05$ (unpaired t-
621 test).

622

623 **Figure 4.** NLRP3 controls the DDR in an inflammasome-independent manner.

624 (**A**) HBEC3-KT control siRNA and caspase-1 siRNA (siCASP1) were treated with Eto 100
625 μM and H2AX phosphorylation was monitored by immunoblot. (**B**) HBEC3-KT control
626 siRNA were treated with the pan caspase inhibitor z-VAD-fmk (50 μM) or the caspase-1
627 inhibitor z-YVAD-fmk (50 μM) 30 min before HU treatment (2 mM, 16 h) and H2AX
628 phosphorylation was analyzed by immunoblotting. (**C**) HBEC3-KT transfected with control
629 or NLRP3 siRNA were treated with IR 2 Gy or (**D**) HU 2 mM for the indicated times and IL-
630 1β was quantified in cell supernatants using a Luminex assay. The line indicates the detection
631 limit. (**E**) HBEC3-KT cells were treated with Eto 100 μM over time and caspase-1 cleavage
632 was analyzed by immunoblot. Actin was used as loading control. These data are from one
633 representative experiment out of two independent experiments. n.d.: not detected

634

635 **Figure 5.** NLRP3 forms a complex with ATM.

636 (**A**) mcherry-NLRP3 and Flag-ATM co-immunoprecipitate in HeLa cells.
637 Immunoprecipitates (IP) and input were analyzed by immunoblotting. (**B**) HeLa cells
638 expressing Flag-NLRP3 were treated or not with Eto for indicated time points. Co-

639 immunoprecipitation of endogenous ATM was analyzed by immunoblotting. **(C)** Different
640 flag-tag NLRP3 domain constructs were transfected in HeLa cells, and Flag-proteins were
641 immunoprecipitated and pull-downed proteins were analyzed by immunoblotting. **(D)**
642 Proximity Ligation Assay was performed in HBEC3-KT cells treated or not with Eto using
643 anti-ATM and anti-NLRP3 (x40). Hoechst (blue) was used to stain nuclei. Scale bars 50 μ m
644 Signal quantification is shown on the graph on the right panel. NT: not treated.

645

646 **Figure 6.** The absence of NLRP3 confers resistance to acute genotoxic stress.

647 **(A and B)** HBEC3-KT transfected with the indicated siRNA were treated with Eto and **(A)**
648 caspase-3/7 activity was then measured by luminometry and **(B)** cell survival by cristal violet
649 cytotoxicity test. **** P < 0.0001, ** P = 0.0046 (unpaired t-test). Results are representative
650 of three experiments. **(C)** *NOXA* and *PUMA* expression were assessed in HBEC3-KT treated
651 with Eto at the indicated time points by Q-RT-PCR relative to *HPRT1* expression. **** P <
652 0.0001, ** P = 0.0035 (multiple comparisons for two-way ANOVA). **(D)** *NOXA* expression
653 was assessed by immunoblotting. Actin was used as a loading control. Representative of two
654 independent experiments.

655

656 **Figure 7.** NLRP3 expression is reduced in human NSCLC compared to healthy tissue.

657 **(A)** Protein levels of the NLRP3 inflammasome components NLRP3, caspase-1 and ASC
658 were assessed by immunoblotting and **(B)** relative *NLRP3* mRNA by Q-RT-PCR in HBEC3-
659 KT cells and in a panel of NSCLC cell lines. Results are representative of more than three
660 experiments. **(C)** Relative *NLRP3* mRNA levels were determined by Q-RT-PCR in a cohort
661 of non-treated primary tumors from NSCLC patients (n = 20) and the corresponding normal
662 lung tissues (n = 10). Data represent mean \pm SEM; *** P < 0.001 (t-test). Kaplan-Meier plots
663 of patients overall survival **(D)** and progression free interval **(E)** in TCGA-LUAD dataset

664 according to NLRP3 expression levels; patients were stratified according to the cutoff
665 obtained from maximally selected rank statistic.

666

667 **Supplementary Figure 1.** HBEC3-KT cells express a functional NLRP3 inflammasome.

668 (A) Immunoblot controlling the efficacy of the siRNA targeting NLRP3 (siNLRP3) against
669 non-targeting siRNA (siCTL) of the HBEC3-KT irradiated cells. Actin was used as a loading
670 control. (B and C) Representative pictures of HBEC3-KT cells transfected with control or
671 NLRP3 siRNA and treated with 2 Gy for 1 h to assess MDC1 (B) or 53BP1 (C) foci
672 formation was analyzed by IF. (x60), Hoechst (blue) was used to stain nuclei. Scale bars 10
673 μm . (D) Scheme displaying the hypothesis used for mathematical modeling of ATM and
674 NLRP3 interactions showing the two hypotheses were investigated A) NLRP3 enhances
675 ATM activation, B) NLRP3 inhibits ATM deactivation.

676

677 **Supplementary Figure 2.** ATM activity is impaired in the absence of NLRP3 in response to
678 DNA damaging agents.

679 (A) HBEC3-KT siRNA-transfected cells were treated with 2 mM HU. At indicated time
680 points, cells were lysed and protein extracts analyzed by immunoblotting for NLRP3, γH2AX
681 (S139), P-p53 (S15), P-KAP1 (S824). Actin was used as a loading control. (B to D) HBEC3-
682 KT cells transfected with control or NLRP3 siRNA were treated with (B) 0.5 μM etoposide
683 for 4 h and P-ATM foci were quantified, and (C) 100 μM Eto and mean fluorescence
684 intensity was quantified in the nucleus, (D) 0.5 μM etoposide for 4 h and γH2AX foci
685 quantified. (x60), Hoechst (blue) was used to stain nuclei. Data represent mean \pm SEM; ***
686 $0.001 < P$ (unpaired t-test). Scale bar 10 μm (E) ROS measurement was performed on
687 HBEC3-KT cells transfected with control or NLRP3 siRNA using DCFDA probe in presence
688 or in absence of 5 μM ATMi KU5593. One representative experiment out of 3.

689

690 **Supplementary Figure 3.** NLRP3 re-expression in tumoral cell lines facilitates ATM-
691 dependent DNA damage signaling.

692 A549 (**A** and **B**) or H292 (**C** and **D**) stably expressing a doxycycline-inducible NLRP3
693 lentiviral vector treated or not with 0.5 μ M of doxycycline were irradiated with 2 Gy for 1 h.
694 Representative pictures of P-ATM (**A** and **C**) and γ H2AX (**B** and **D**) IF staining that was
695 quantified in Figure 3 A to D. (x60), Hoechst (blue) was used to stain nuclei. Scale bars 10
696 μ m. (**E**) H520 cells stably expressing the NLRP3 or CTL vector were treated with 0.5 μ g/mL
697 of doxycycline 24 h before irradiation with 6 Gy. At indicated time points, cells were lysed
698 and protein extracts analyzed for NLRP3, γ H2AX (S139), P-KAP1 and KAP1 by
699 immunoblotting. Actin was used as a protein loading control.

700

701 **Supplementary Figure 4.** NLRP3 is localized in the cell cytosol and nucleus, but most
702 NLRP3/ATM complexes are present in the cell cytosol.

703 (**A**) HBEC3-KT untreated (0) or irradiated (2 Gy) were separated and proteins from the
704 cytosolic (C) and nuclear (N) fractions were analyzed by immunoblot. Tubulin was used as a
705 marker of the cytosolic fraction and fibrillarin of the nuclear fraction. T is total lysate. (**B**)
706 Confocal images illustrating the cellular localization of the different NLRP3 domains
707 transfected in HeLa cells (x63). Hoechst (blue) was used to stain nuclei. (**C**) NLRP3 is
708 detected in the cytosol and the nucleus compartment in live confocal image of mCherry-
709 NLRP3 transfected in H292 cells. (**D**) Proximity Ligation Assay in HeLa cells transfected
710 with an empty vector or a NLRP3-expressing vector using anti-ATM and anti-NLRP3
711 antibodies (x40). Hoechst (blue) was used to stain nuclei.

712

713 **Supplementary Figure 5.** NLRP3 silencing decreases nuclear ATM.

714 (A and B) HBEC3-KT sh control cells or knocked down for NLRP3 were left untreated (A) or
715 irradiated at 2 Gy for 1 h (B). Total ATM was stained for immunofluorescence and the mean
716 fluorescent intensity was quantified. Results are representative of two independent
717 experiments (x60). Hoechst (blue) was used to stain nuclei. Scale bar 10 μ m.

718

719 **Supplementary Figure 6.** NLRP3 does not control the extrinsic apoptosis pathway.

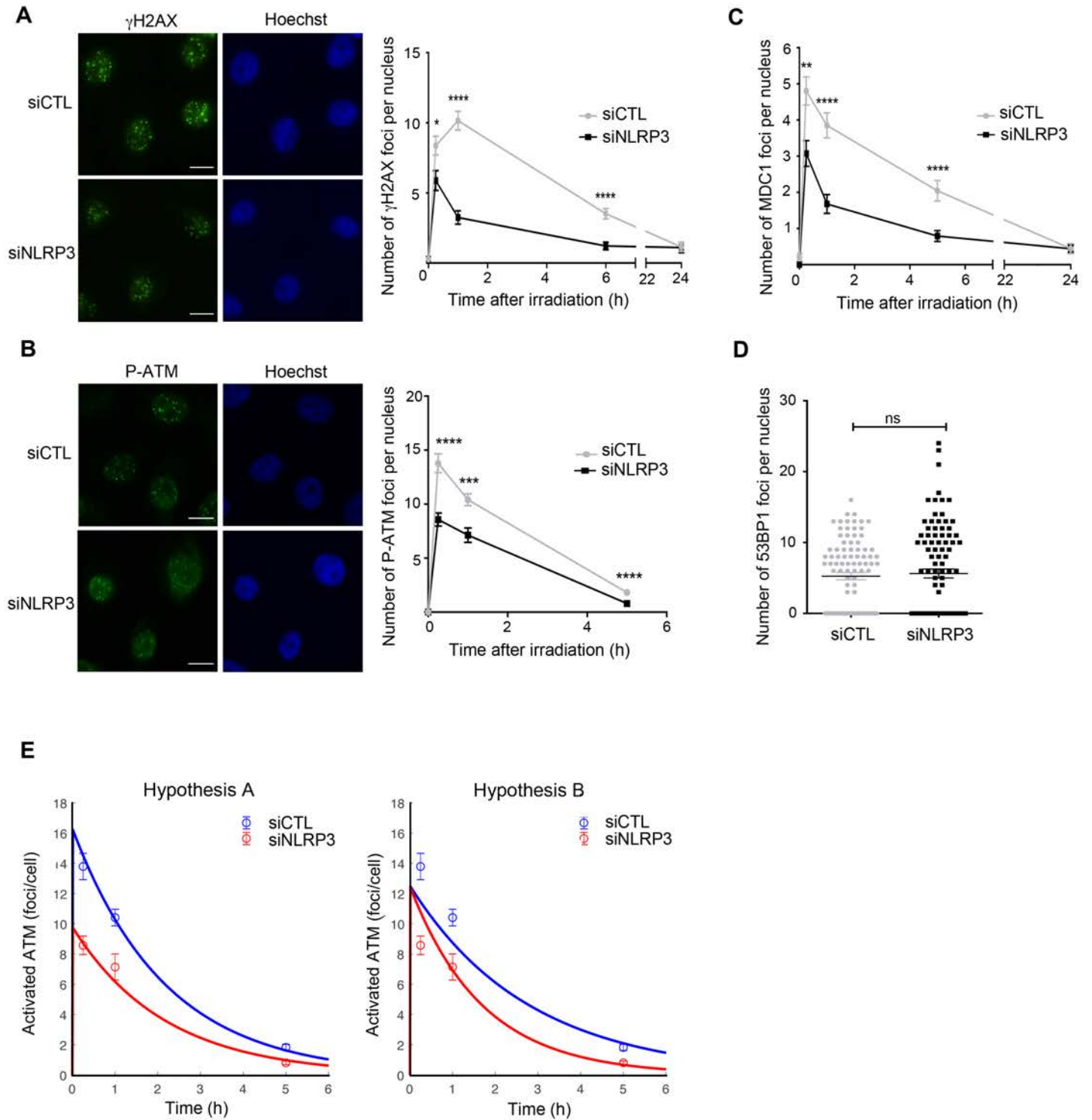
720 (A) HBEC3-KT cells transfected with control or NLRP3 siRNA were treated with Trail 200
721 ng/mL and MG132 1 mM for 12 h to induce death receptor-mediated apoptosis. Data
722 represent mean \pm SEM; ns: not significant (t-test). (B) Model of resistance to genotoxic stress
723 caused by reduced NLRP3 expression. DNA DSBs activate the ATM kinase which
724 phosphorylates many protein substrates involved in the control of the outcome to genotoxic
725 stress. Down-regulation of NLRP3 impairs ATM activation resulting in decreased levels of
726 phosphorylation of several ATM substrates, including p53, thus promoting cell survival.

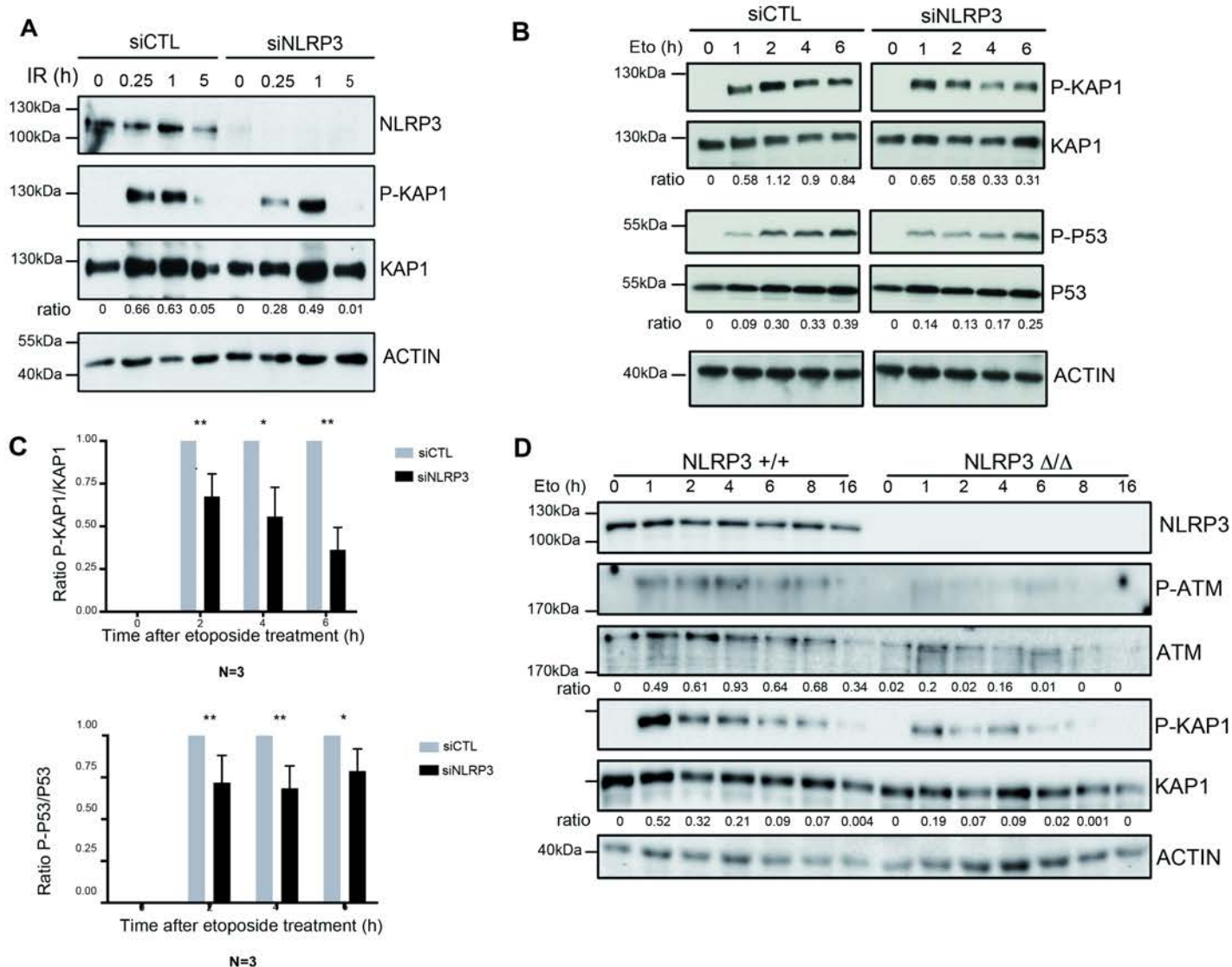
727

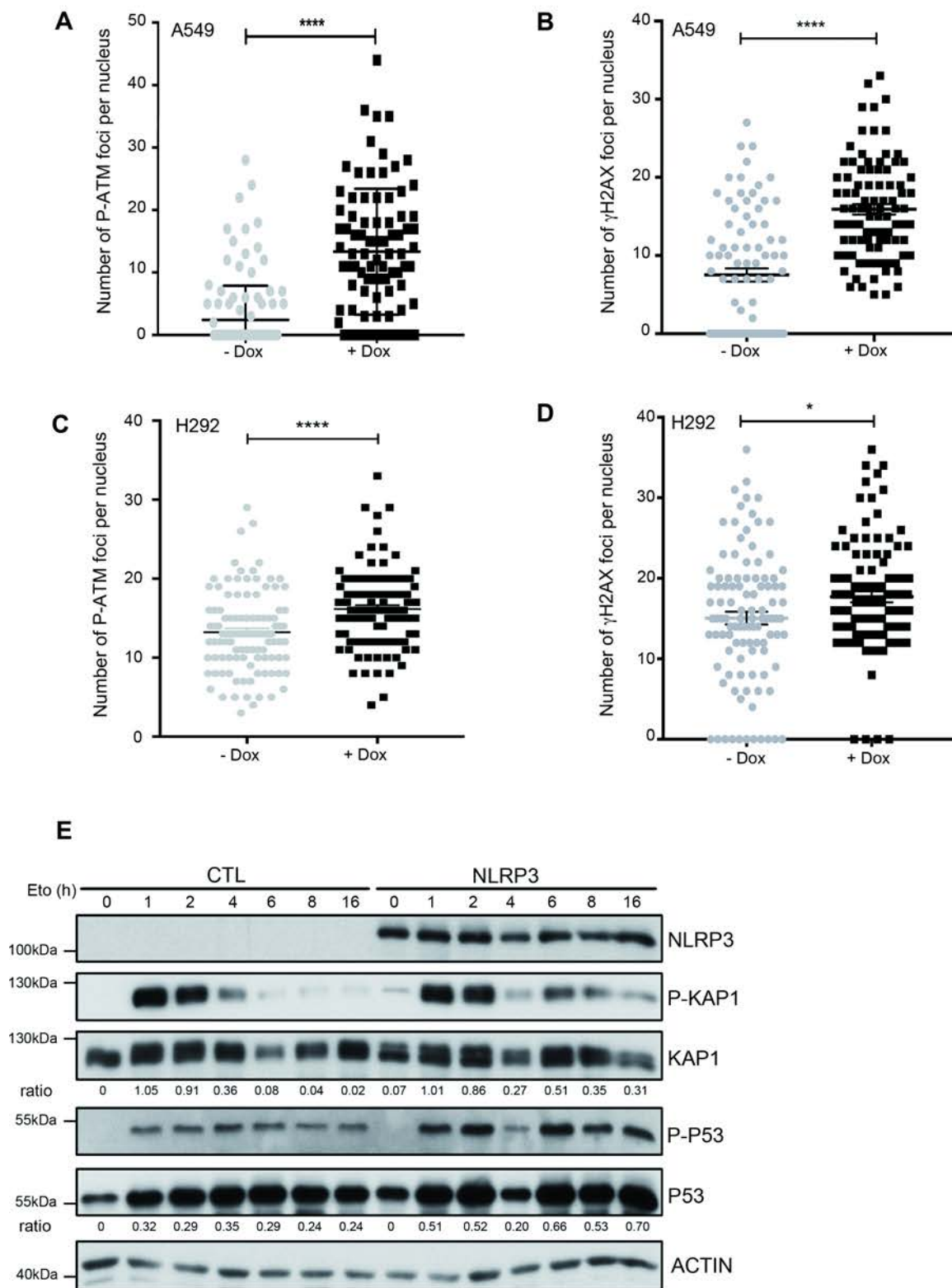
728 **Supplementary Figure 7.** NLRP3 expression is reduced in human NSCLC compared to non-
729 tumoral cells.

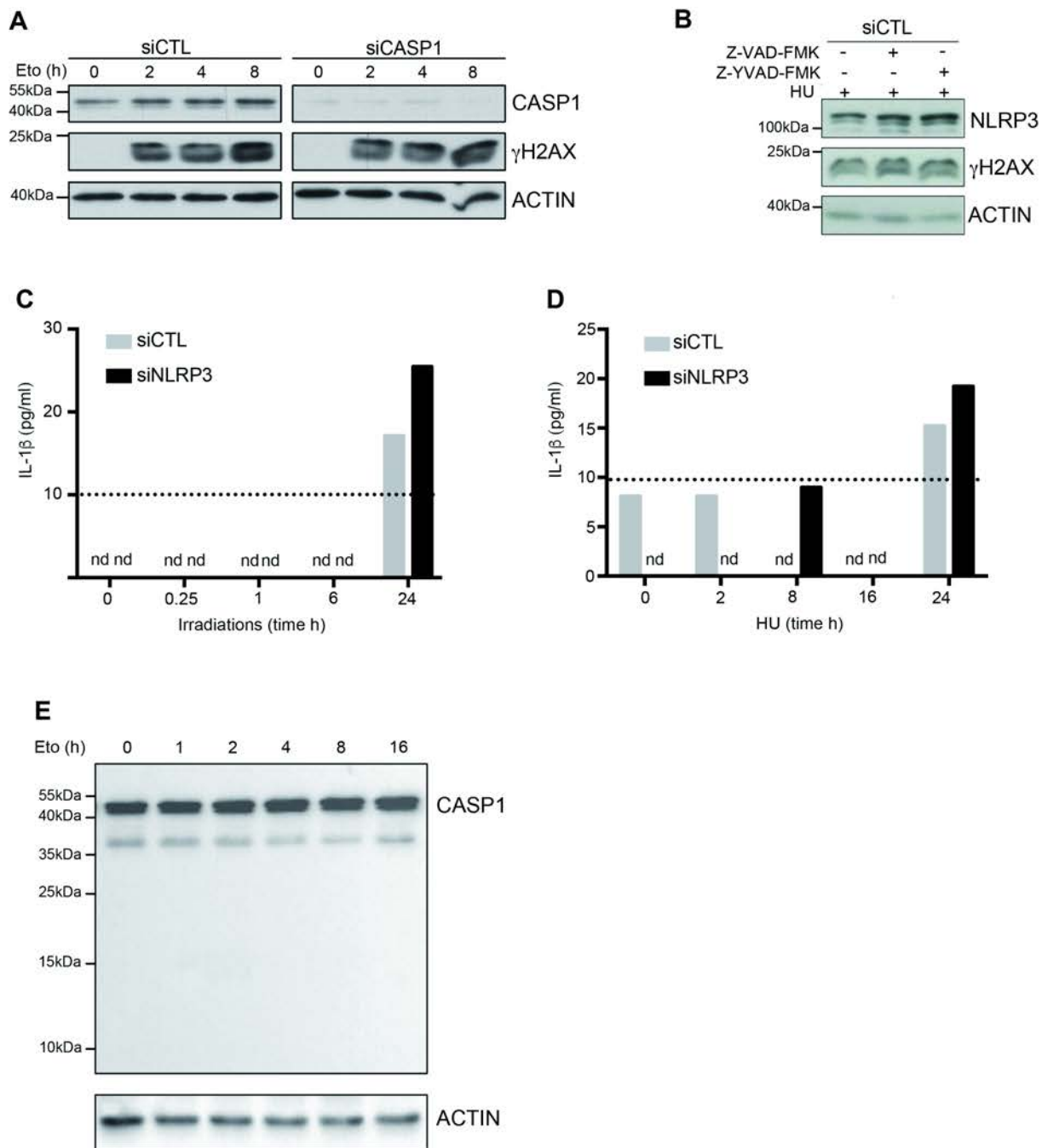
730 (A) NLRP3 inflammasome components, namely NLRP3, caspase-1 and ASC were assessed by
731 immunoblotting in NSCLC cell lines. GADPH was used as a protein loading control. (B)
732 Anchorage-independent growth ability was assessed in HBEC3-KT cell lines.

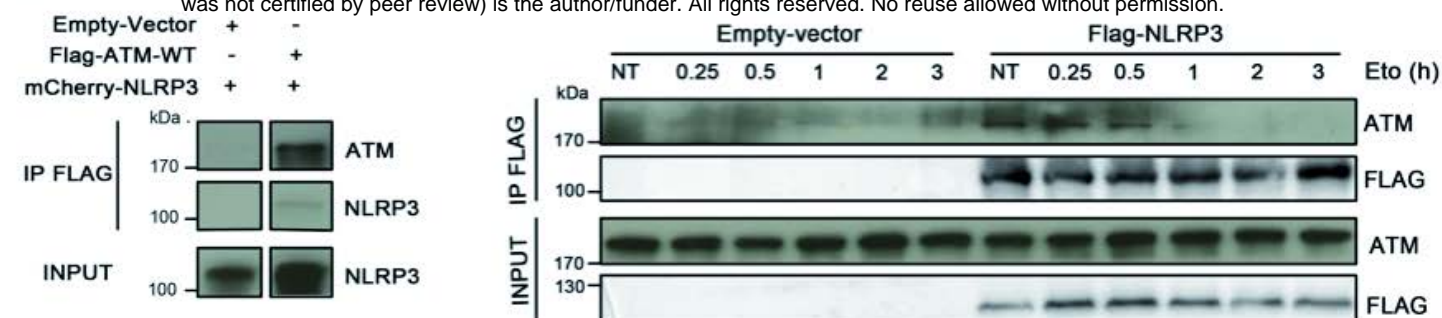
733



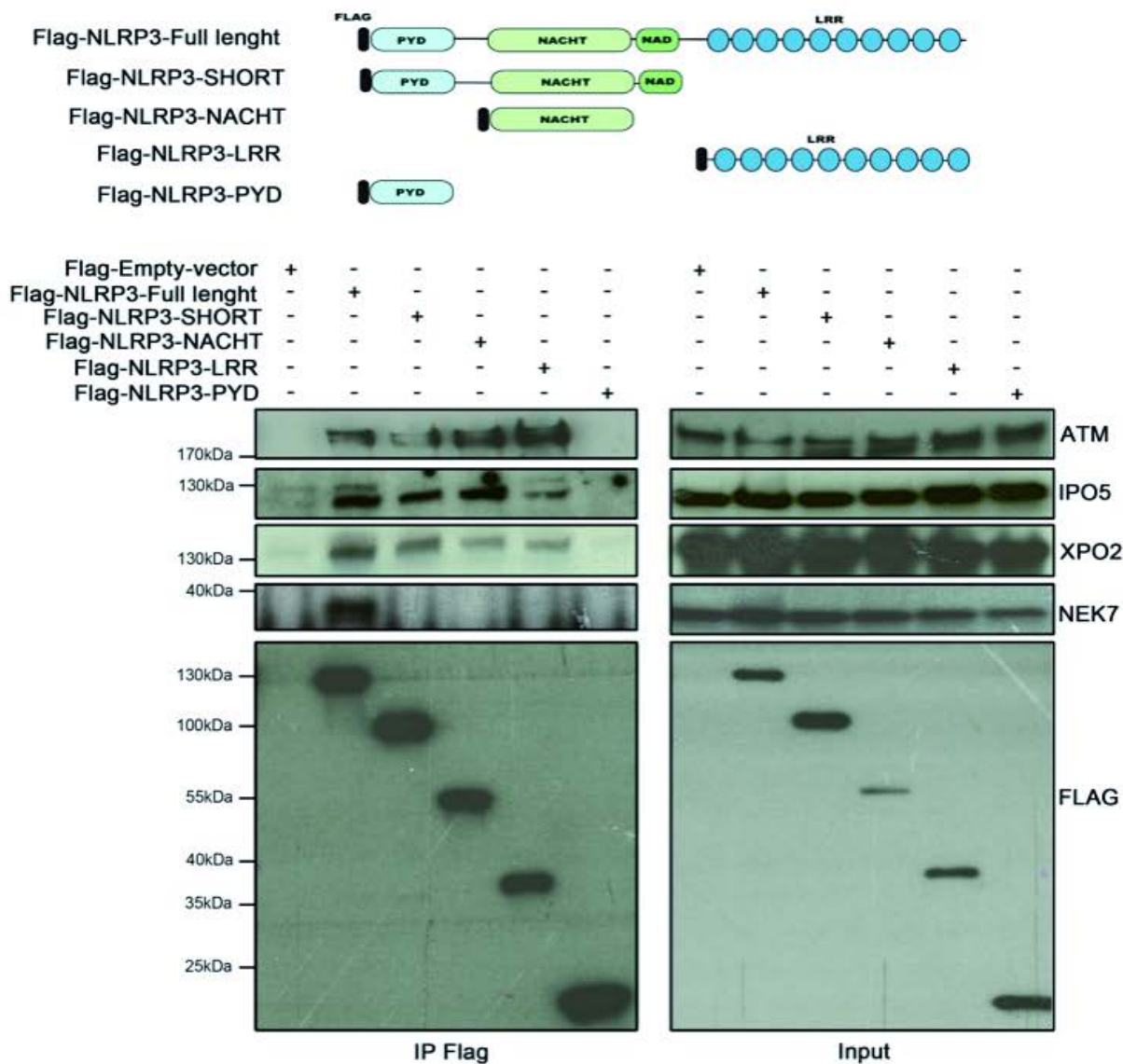








C



D

